Design and Operational Considerations of Catalytic Membrane Reactors for Ammonia

Synthesis

Zhenyu Zhang, J. Douglas Way, Colin A. Wolden*

Department of Chemical and Biological Engineering, Colorado School of Mines, Golden,

Colorado 80401, United States

Abstract

Production of ammonia using hydrogen derived from renewable electricity instead of hydrocarbon reforming would dramatically reduce the carbon footprint of this commodity chemical. Novel technologies such as catalytic membrane reactors may potentially be more compatible with distributed ammonia production than the conventional Haber-Bosch process. A reactor model is developed based on integrating a standard industrial iron catalyst into a catalytic membrane reactor (CMR) equipped with an inorganic membrane that is selective to NH₃ over N₂/H₂. CMR performance is studied as functions of wide ranges of membrane properties and operating conditions. Conversion and ammonia recovery are dictated principally by the ammonia permeance, and the benefits by using membranes become significant above $100 \ GPU = 3.4 \times 10^{-8} \ mol \ m^{-2} \ s^{-1}$ Pa^{-1} . To be effective, the CMR requires a minimum selectivity for ammonia of 10 over both nitrogen and hydrogen, and purity scales with the effective selectivity. Increasing the pressure of operation significantly improves all metrics, and at $P = 30 \, bar$ with a quality membrane ammonia is almost completely recovered, enabling direct recycle of un-reacted hydrogen and nitrogen without need for recompression. Temperature drives conversion and scales monotonically without thermodynamic limitations in a CMR. Alternatively, the temperature may be reduced as low as $300^{\circ}C$ while achieving conversion levels surpassing equilibrium limits at T = $400^{\circ}C$ in a conventional reactor.

1

Introduction

Renewables accounted for 25.2% of global electricity generation in 2018, and are the fastest growing technologies for new deployment with wind and photovoltaics increasing by 23.0% and 36.5%, respectively. Renewable power generation is inherently distributed and variable, 2 necessitating efficient energy storage and transportation solutions. The electric grid and battery storage are useful for short term management, but suffer from challenging integration issues and limited capacity.² Chemical storage is attractive for medium- and long-term storage. The simplest electrochemical conversion is hydrogen generation through electrolysis of water, but hydrogen storage and transportation is itself a very formidable task. Currently, hydrogen is stored via cryogenic condensation and/or compression up to 700 bar. Both approaches suffer from low volumetric density and boil-off, putting practical constraints on both the duration and distance associated with these approaches.³ Conversion to ammonia has emerged as a promising energy vector for hydrogen storage and transportation. Its gravimetric and volumetric hydrogen density are 17.7 wt.% and 108 g/L, respectively. Additionally, ammonia is a major commodity chemical (> 175 million metric tons (MMT)/year) with an existing global infrastructure for distribution and regulation in place.⁴ Conventionally, ammonia synthesis is conducted using the Haber-Bosch process at extreme pressures (100 - 200 bar) in centralized facilities where hydrogen is predominantly supplied by reforming hydrocarbons, making it the leading commodity chemical in terms of energy consumption and greenhouse gas emission. 5 A transition to green ammonia derived from renewable hydrogen would be desirable to both displace current production and additionally serve as a vector for renewable hydrogen distribution. Capital-intensive Haber-Bosch is not economical at small scale, so there is need to develop modular technologies for distributed production that would be more compatible with renewable resources.⁶

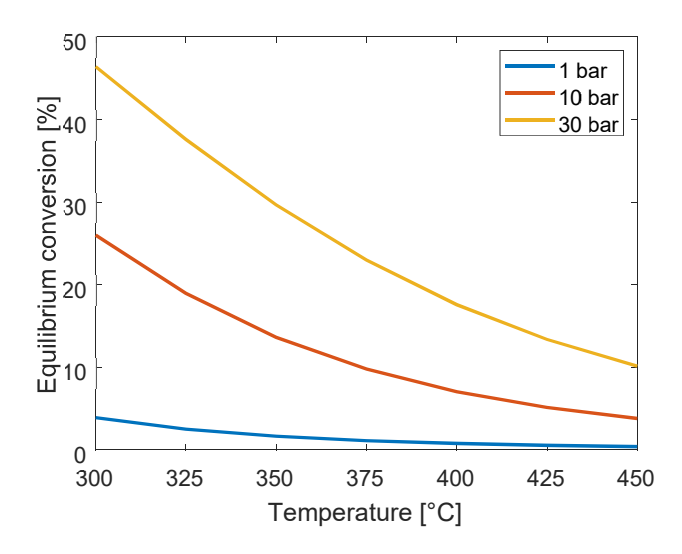


Figure 1: Equilibrium conversion of stoichiometric N₂:H₂ mixtures as a function of temperature at selected pressures

Reducing the capital intensity of ammonia synthesis requires development of processes that operate at milder combinations of temperature and pressure. Currently the reaction is conducted in a packed bed reactor with conversion approaching equilibrium limits at $T \sim 450^{\circ}C$. The effluent is cooled to $T \sim -25^{\circ}C$ to condense and recover ammonia, and the unreactive gasses are recompressed, reheated, and recycled to the reactor. There has been a century of effort to develop catalysts that are more active at lower temperature, as that would greatly reduce thermodynamic constraints (Figure 1). There have been numerous reports displaying high activity in differential reactors, but these catalysts are often inhibited by hydrogen and/or ammonia and their performance under practical conditions is not significantly improved over the commercial wustite catalysts.⁷⁻⁹ A second strategy is to improve the separation process. Cussler and co-workers have championed novel absorbents as a cost–effective alternative to conventional condensation.¹⁰⁻¹² Perhaps the best opportunity are processes that integrate reaction and separation.^{13,14} Catalytic membrane reactors (CMRs) offer process intensification by combining reaction and separation into a single unit. In

addition to the compact and modular design, efficient product removal relaxes both thermodynamic limitations and kinetic inhibitions.

In this paper, we explore the potential of CMR technology for ammonia synthesis at moderate operating conditions. The model of CMR incorporates a conventional iron catalyst with membranes of variable permeance and selectivity. Here we aim to elucidate the CMR performance dependence on the ammonia membrane properties using a reactor model, and in doing so establish minimum requirements for permeance and selectivity that would enable this application. Key performance metrics include conversion, ammonia recovery, and the ammonia purity in both the permeate and the retentate. The sensitivity to operating conditions are also explored to illustrate the potential benefits of a CMR over a conventional packed bed reactor.

Reactor model development

Kinetics of bulk iron catalysts

The Haber-Bosch process uses bulk iron catalysts typically promoted with three non-reducible metal oxides. For example, the KM1 catalyst by Haldor Topsøe A/S is comprised of 94% iron, 2.8% calcium oxide, 2.5% aluminum oxide, and 0.6% potassium oxide. Sehested et al. Validated a global rate expression (Eq. 2) with high fidelity using experimental results of the KM1R catalyst over extensive conditions where T = 320 - 440°C, $P = 1 - 100 \ bar$, space velocity = 12,000 - 120,000 $mL \ gcat^{-1} \ h^{-1}$. Additionally, a good fit is realized by comparing kinetic model predictions with wide-ranging experimental results of both Nielsen et al. Additional Kowalczyk.

$$r = 2N_s K_1 k_2 \theta_*^2 \left(P_{N_2} - \frac{P_{NH_3}^2}{P_{H_2}^3 K_{eq}} \right)$$
(1)

$$\theta_* = \left(1 + \frac{P_{NH_3}}{P_{H_2}^{1.5} K_a} + \frac{P_{H_2}^{0.5}}{K_b}\right)^{-1} \tag{2}$$

The mechanism of the global synthesis reaction consists of four elementary steps including nitrogen adsorption (denoted using subscript 1), nitrogen dissociation (2), hydrogen adsorption and dissociation (*b*), and surface reaction (*a*). The nitrogen dissociation step is assumed to be the rate limiting step. r is the ammonia synthesis rate. N_s is the active sites density. K_1 is the equilibrium constant for the nitrogen adsorption step. k_2 is the forward rate constant for the nitrogen dissociation step. θ_* is the fraction of the surface coverage for free sites. K_{eq} is the equilibrium constant for the global reaction. K_a is the equilibrium constant for the surface reaction step. K_b is the equilibrium constant for the hydrogen adsorption and dissociation step. Table 1 summarizes the kinetic parameters in Eq. 2, which are in an Arrhenius form as

$$A \exp\left(\frac{-E_a}{RT}\right)$$

Table 1: Summary of kinetic parameters including values and units for Eq. 2

Kinetic	Units	Pre-exponential factor A	Activation energy E_a
parameters			$[kJ mol^{-1}]$
$2NsK_1k_2$	$[\mu mol\ gcat^{-1}\ s^{-1}\ bar^{-1}]$	7.80×10^{3}	6.6
K_{eq}	$[bar^{-2}]$	2.03×10^{-12}	-101.6
K_a	$[bar^{-0.5}]$	2.73×10^{-2}	27.1
K_b	$[bar^{0.5}]$	2.16×10^{3}	48.0

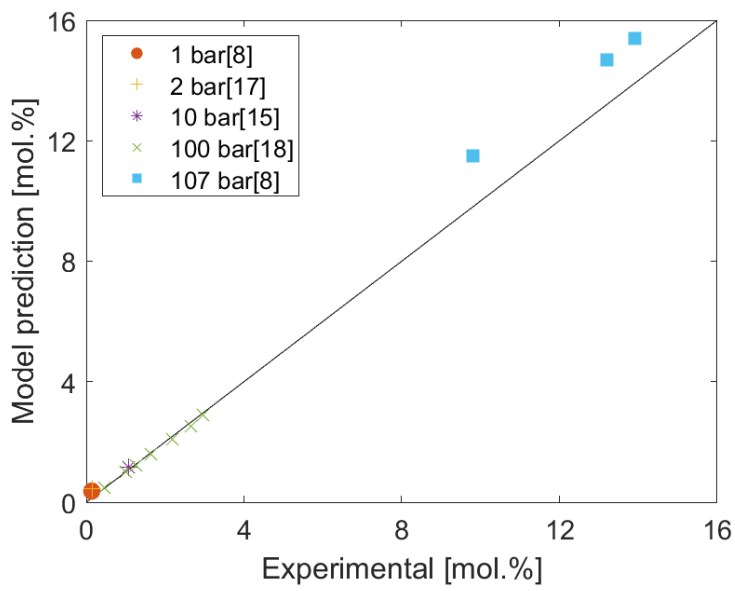


Figure 2: Comparison of ammonia outlet concentration in an integral reactor between experimental results and model predictions of bulk iron catalysts at $T = 400^{\circ}C$ and $P = 1 \ bar^{8}$, $2 \ bar^{17}$, $10 \ bar^{15}$, $100 \ bar^{18}$, $107 \ bar^{8}$.

To further validate this rate expression for use in our CMR simulations, we built a differential rate calculator using kinetics parameters from Sehested et al. 16 and tested its ability to reproduce a number of packed bed reactor experiments reported in the literature. Figure 2 summarizes a comparison of model predictions of ammonia outlet concentration with literature results for integral reactors operated at $T = 400^{\circ}C$ and P = 1 - 107 bar. Excellent agreement is achieved over a broad range of conditions, with minor discrepancies observed at extreme conditions that are not pertinent to the current study (1 and $107 \ bar^8$). The reasons for such discrepancy remain unclear. For the conditions targeted for CMR operation, $10 - 30 \ bar$ and modest conversion, the model works extremely well. A more extensive review of the ammonia catalyst literature and additional validation of the rate expression employed is presented in the Supporting Information.

Reactor model

The CMR module is assumed to have the same design as documented in Collins and Way. ¹⁹ Briefly, the reactor is comprised of an ammonia permeable membrane deposited on the exterior of a tubular support with bulk iron catalyst packed in the lumen. The reactor is assumed to operate at steady state, isothermal, and isobaric conditions. Thus, only the mass conservation needs to be solved. Additionally, the reactor model is assumed to be 1D, i.e., no species variation in the radial direction. The validity of this assumption is examined using the criteria modified from Raja et al. ²⁰ as follows.

$$\frac{r}{L} \ll Re_r Sc \ll \frac{L}{r} \tag{3}$$

Where r and L are the radii and the length of the tubular reactor, separately. Re_r is the Reynolds number based on the radii of the reactor. Sc is the Schmidt number. Operating within these bounds ensures that convection is fast relative to diffusion in the axial direction but slow enough that there the system is well mixed in the radial direction. The permeation flux per volume, i.e., the packing density of tubular membranes, inversely scales with the radius, at fixed ammonia permeance, and pressure driving force. Based on our previous work on with CMRs^{7,21} a typical L/r ratio is 40. Here we assume L and r are 20 cm and 0.5 cm, respectively. This sets the valid GHSV in the range of \sim 8 - 12,800 h^{-1} . The packed iron catalyst implements a kinetics expression (eq. 2) as discussed above. The catalyst density is assumed to be 4.8 g/cm^3 . The porosity of the catalyst and the catalyst bed voidage are 0.44^{22} and 0.33^{23} , respectively. A summary of the model input parameters is given in Table 2.

Table 2: Summary of the reactor model setup.

Parameters	Values		
L[cm]	20		
r[cm]	0.5		
Permeation area $A_m[cm^2]$	62.8		
Valid GHSV range $[h^{-1}]$	8 - 12,800		
Catalyst density [g cm ⁻³]	4.8		
Catalyst porosity	0.44		
Catalyst bed voidage	0.33		

A list of the governing equations is briefly summarized as follows. A more detailed derivation can be found in the supplemental information MatLab script.

$$\frac{\partial(\rho u)}{\partial z} = -F_{m/g} \sum_{k=1}^{K_g} J_k W_k \tag{4}$$

$$\frac{\partial(\rho_k u)}{\partial x} = \gamma_k r_{NH_3} W_k - F_{m/g} J_k W_k \tag{5}$$

$$\frac{\partial(\rho_k u)}{\partial z} = \gamma_k r_{NH_3} W_k - F_{m/g} J_k W_k
\rho = \frac{P}{RT} \frac{1}{\sum_{k=1}^{K_g} Y_k / W_k}$$
(5)

$$J_k = \kappa \Delta P_k = \kappa (P_{k,ret} - P_{k,per}) \tag{7}$$

The overall continuity equation is given as eq. 4. The net change of mass fluxes is equal to the permeation fluxes through the membrane. The net change of mass fluxes due to reactions equals to zero. $F_{m/g}$ is a factor that represents the ratio of the surface area of the membrane to the volume of the reactor. W_k is the molecular weight of species k, and J_k is the permeation flux of species k by membrane separation. The species continuity equation 5 has an additional reaction term $\gamma_k r_{NH3}$ representing the species mass flux by the synthesis reaction, where γ_k is the stoichiometric coefficient of species k. Eq. 6 is the gas model approximated using the ideal gas law, where Y_k is the mass fraction of species k. Eq. 7 gives the relation between the permeation flux J_k and the

membrane permeance κ and the pressure driving force. Here we assume vacuum conditions on the permeate side for simplicity.

The performance of the CMR synthesis is evaluated against the conventional process using metrics such as the conversion, ammonia recovery, and permeate and retentate ammonia purity. The conventional packed bed reactor (PBR) counterpart is assessed at conditions with no permeation. The ammonia permeable membrane is characterized using ammonia permeance (κ), ammonia over nitrogen (A/N) selectivity (S), and ammonia over hydrogen (A/H) selectivity (S). The parameter space explored is summarized in the Table 3. Operating conditions include temperature (250 - 450°C), pressure (10 - 30 bar), space velocity (1000 - 8000 h^{-1}), H₂/N₂ ratio (β = 3). Membrane properties include NH₃ permeance (10 - 1000 GPU, where 1 GPU = 3.4 × 10⁻¹⁰ $mol\ m^{-2}s^{-1}Pa^{-1}$), A/N selectivity (1 - 1000), A/H selectivity (1 - 1000).

Table 3: Summary of the parameter space.

Values
250 - 450
10 - 30
3
1000 - 8000
10 - 1000
1 - 1000
1 - 1000

Results and discussion

The Haber-Bosch process is typically conducted by approaching equilibrium conversion in a reactor followed by separation using a condenser and recycling unreacted N₂ and H₂. Extremely high reactor pressures are employed (100 - 200 *bar*) to maximize the level of equilibrium conversion. In contrast, the CMR process removes ammonia while the synthesis reaction happens. This alleviates both the strong ammonia inhibition of the synthesis kinetics and thermodynamic limitations. The ammonia removal by membrane separation can also generate a permeate stream with higher ammonia concentration, which makes the subsequent ammonia purification more cost-effective. The goal of this work was to explore a wide parameter space including the operating conditions and membrane properties and their effects on the interplay between kinetics, thermodynamics, and permeation.

First, to balance between high ammonia production rate and high ammonia outlet concentration for separation, an appropriate gas hourly space velocity (GHSV) needs to be selected using a conventional PBR at $T = 400^{\circ}C$. Figure 3 plots the conversion versus pressure at selected values of GHSV. For GHSV $\leq 1000 \text{ h}^{-1}$ equilibrium conversion is obtained and the level of conversion gradually decreases with increasing GHSV. The conversion maintains over 80% of the equilibrium conversion at GHSV as high as 4000 h^{-1} and pressures up to 30 bar, which is used as the base space velocity in the following discussion. The H_2/N_2 feed ratio is set at 3 in accordance with conventional practice to maximize per pass conversion. Next, we performed CMR simulations for optimized membrane properties including ammonia permeance, A/N, and A/H selectivity and operating conditions including temperature and pressure.

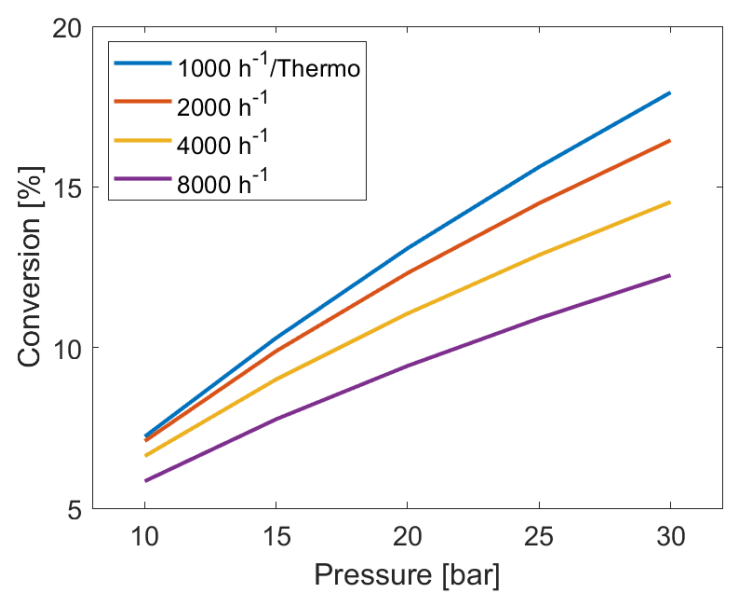


Figure 3: Conversion vs. pressure at various GHSV for the base case of a PBR with no permeation at $T = 400^{\circ}C$. At GHSV $\leq 1000 \text{ h}^{-1}$ equilibrium conversion is obtained.

Role of the Membrane on Conversion

The three critical parameters are the ammonia permeance and its selectivity over both N_2 (A/N) and H_2 (A/H). Conversion is defined as the ratio of the nitrogen consumed by the synthesis reaction to the inlet nitrogen. Figure 4 evaluates the dependence of conversion on ammonia permeance, A/H, and A/N selectivity. As shown in Figure 4 (a), at ammonia permeance of 10 *GPU* the conversion profile is almost constant and close to the conventional PBR regardless of the selectivity values. As the ammonia permeance increases from 10 to 100 *GPU* (Figure 4 (b)), the conversion of a CMR can surpass both the PBR and equilibrium when both the A/N and A/H selectivity are >10. Interestingly, further improvements in selectivity beyond this threshold do not impact conversion, as it plateaus independent of the permeance level. Under these conditions only ammonia is effectively removed and the composition down the length of the reactor remains nearly

constant at the feed ratio of β = 3. When one or both selectivity values fall below this threshold, the composition in the reactor becomes enriched in either hydrogen or nitrogen, resulting in diminished conversion. Conversion is more sensitive to the A/H selectivity than the A/N selectivity, reflecting the inlet mixture stoichiometry. For equivalent permeance values the initial rate of H₂ removal is 3X than N₂ larger due to difference in driving force. This is clearly seen in Fig. 4 (a) and (b). In Figure 4(c) it appears that the results are more sensitive to the A/N selectivity, but this is an artifact because the results are cut off at an A/H selectivity of 5, where it extends down to 1 for A/N selectivity. The significant loss of hydrogen from the system at GPU = 1000 lead to spurious solutions for A/H < 5. With an ammonia permeance of 1000 GPU a conversion of 13.9% is predicted for selectivity values above the critical threshold of 10, almost double the equilibrium conversion. It is noted that high conversion (12.4%) is obtained even with both selectivities as low as 5.

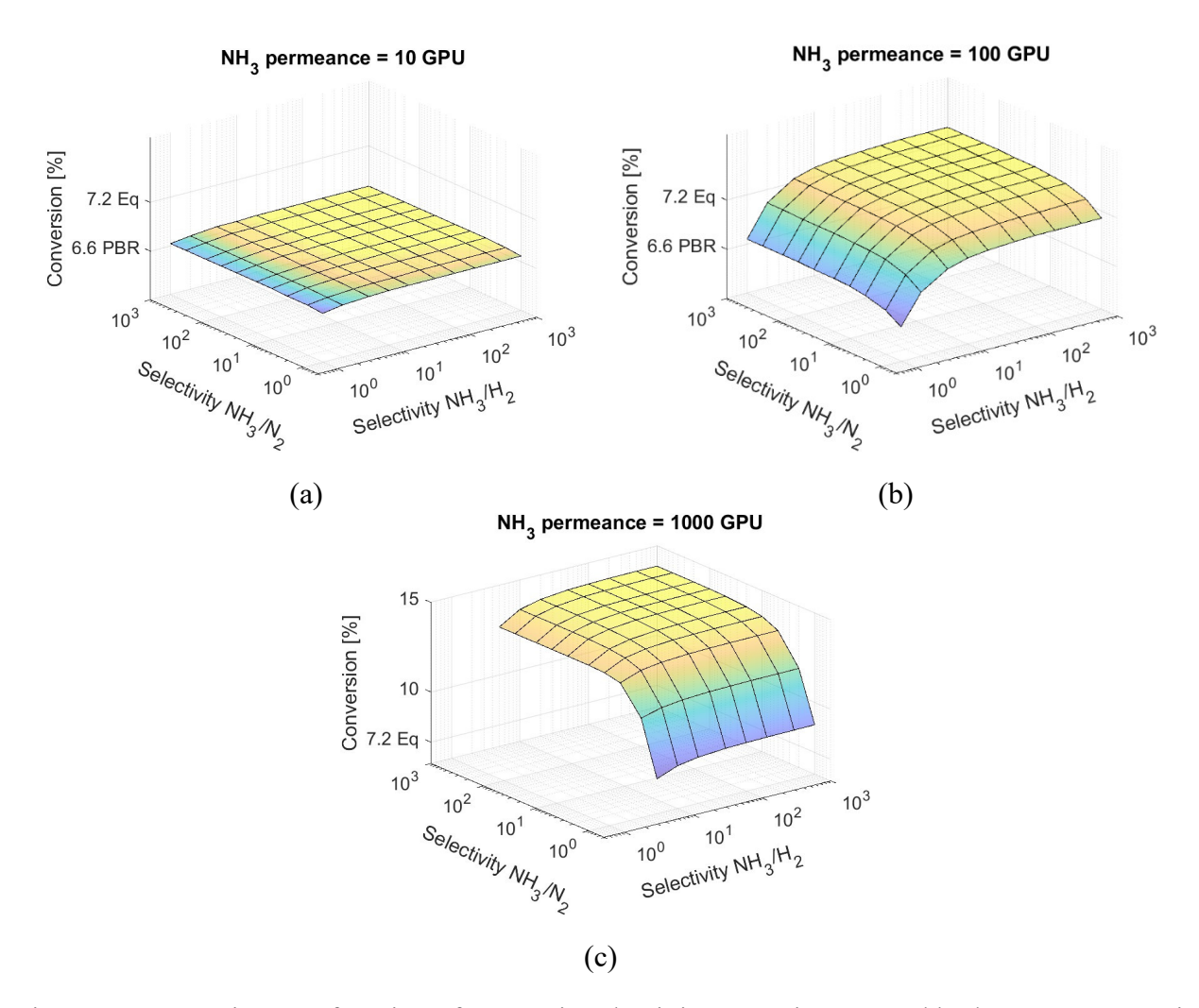


Figure 4: Conversion as a function of ammonia selectivity over nitrogen and hydrogen at ammonia permeance levels of (a) 10, (b) 100, and (c) 1000 *GPU* with other conditions fixed at $T = 400^{\circ}C$, $P = 10 \ bar$, H_2/N_2 ratio = 3, and $GHSV = 4000 \ h^{-1}$. PBR conversion (6.6%) represents the packed bed reactor with no membrane separation. Equilibrium conversion is 7.2% at these conditions. Note that in Fig. 4c the results are cut off below A/H = 5 due to numerical instabilities encountered.

Ammonia recovery

Ammonia recovery is defined as the ratio of ammonia in the permeate stream divided by the ammonia production by synthesis reactions. Figure 5 (a) plots the ammonia recovery profile at the ammonia permeance of 10 GPU. The amount of recovery is negligible (2.3%) and its variation is insensitive to values of A/H and A/N selectivity. As shown in Figures 5 (b) and (c), the recovery values increase from $\sim 2.3\%$ to $\sim 20\%$ and $\sim 75\%$, when the ammonia permeance increases from 10 to 100 and 1000 GPU, respectively. At an ammonia permeance bigger than 100 GPU, the ammonia recovery inversely scales with the A/H and A/N selectivity. This is somewhat misleading. The conversion drops significantly at selectivity values < 10 (Fig. 5), so it is easier to fully recover the limited amount of ammonia produced. However, above the threshold variations in selectivity has little impact on ammonia recovery which is driven primarily by permeance.

The modified Peclet (*Pe*) number (eq. 8) evaluates the potential of the membrane in permeating ammonia, and is defined as the ratio of the maximum quantity of ammonia that can be permeated using the membrane over the maximum quantity of ammonia that can be produced.²⁴

$$Pe = \frac{\kappa \Delta P A_m}{0.5 F_{N_2 + H_2}} \tag{8}$$

Fig. 5 (d) displays the recovery as a function of Pe number on a semi-log scale for various combinations of pressure (10 - 30 bar) and ammonia permeance (10 - 1000 GPU) conditions, assuming perfect A/H and A/N selectivity. There is a sigmoidal variation starting from negligible recover for Pe < 0.1 to nearly complete recovery for Pe > 10. The key factor is the product in the numerator, which shows that deficiencies in permeance may be offset by the reactor aspect ratio (Am) and/or operating conditions (ΔP).

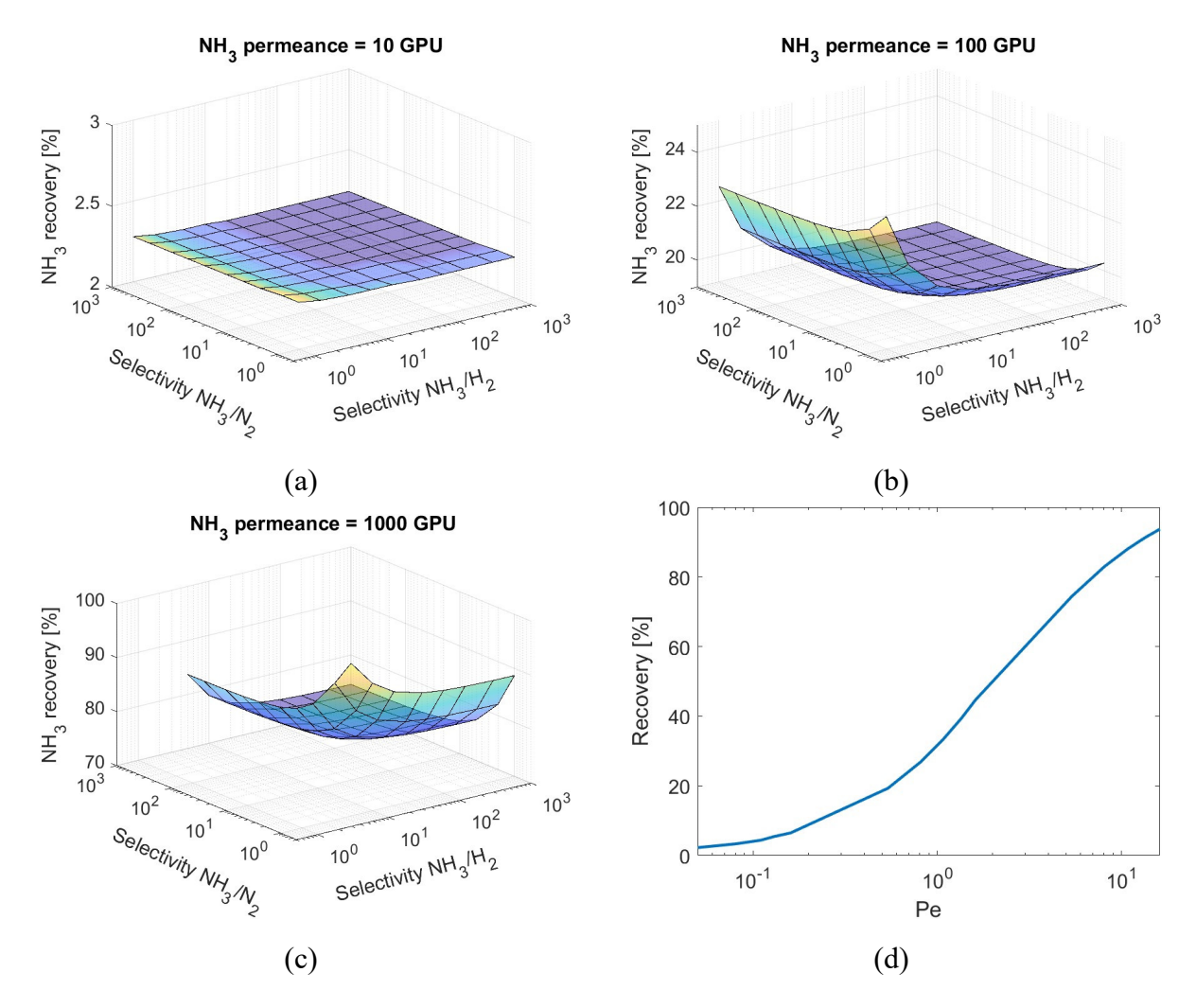


Figure 5: Ammonia recovery as a function of ammonia selectivity over nitrogen and hydrogen at ammonia permeance levels of (a) 10, (b) 100, and (c) 1000 *GPU* with other conditions fixed at T = $400^{\circ}C$, P = $10 \ bar$, H₂/N₂ ratio = 3, and GHSV = $4000 \ h^{-1}$ (d) Ammonia recovery as a function of Pe number assuming perfect A/N and A/H selectivities at T = $400^{\circ}C$, P = $10 - 30 \ bar$, H₂/N₂ ratio = 3, GHSV = $4000 \ h^{-1}$, and ammonia permeance values are within $10 - 1000 \ GPU$.

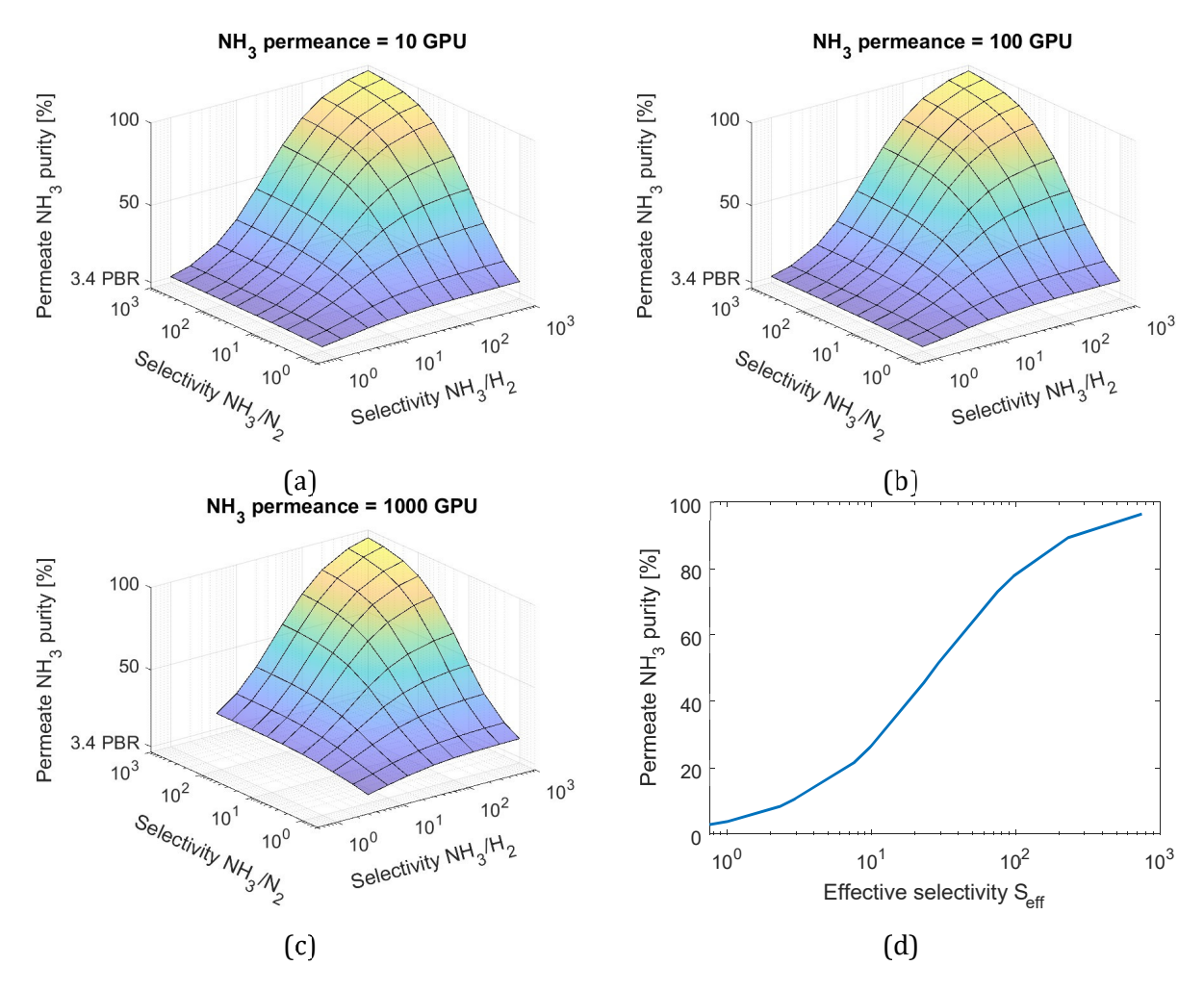


Figure 6: Permeate purity as a function of ammonia selectivity over nitrogen and hydrogen at ammonia permeance levels of (a) 10, (b) 100, and (c) 1000 *GPU* with other conditions fixed at T = $400^{\circ}C$, P = $10 \ bar$, H₂/N₂ ratio = 3, and GHSV = $4000 \ h^{-1}$. The purity exiting a PBR is 3.4% at these conditions. (d) Permeate purity plotted vs. effective selectivity from these simulations (a-c).

Ammonia Purity

The purity of the ammonia recovered from the permeate defines the size of a subsequent condenser as well as the subsequent recycle stream. Figure 6 plots the ammonia purity in the permeate stream at various A/N and A/H selectivity values. The profile is essentially independent of the ammonia permeance. The level of conversion and recovery were largely independent of selectivity as long as the values were above the threshold of 10. In contrast, permeate purity is strongly dependent on the selectivity, scaling with the logarithm of an effective selectivity (Fig. 6 d), which is defined as:

$$S_{eff} = \frac{S_{A/N}S_{A/H}\beta}{S_{A/H} + S_{A/N}\beta(9)}$$

where β is the H₂:N₂ ratio. The effective selectivity is controlled by the lower of two selectivities. For example, if one of the selectivities is unity, improving the other does little to improve purity. For stoichiometric mixture ($\beta = 3$) the A/H selectivity is more important than the A/N selectivity. Compared to the PBR scenario, the use of CMR can upgrade the ammonia fraction from 3.4% to > 22% if the A/H and A/N selectivity are equal to 10.

Pressure and temperature dependence

We have also evaluated the CMR performance as a function of temperatures (250 - 450°C) and pressure (10 - 30 bar). To illustrate the important trends we display results at fixed membrane properties including the ammonia permeance = 1000 GPU, A/H selectivity = 10, and A/N selectivity = 100. The higher A/N selectivity reflects the expectation that the larger N₂ molecule will be more easily separated by a size exclusion transport mechanism. Other membrane materials with different mechanisms such as solution diffusion of a facilitated transport could potentially achieve higher A/H selectivities. Figure 7 compares the conversion of a CMR, PBR, and equilibrium as a function of pressure at T = 400°C. Conversion in the CMR increases linearly with pressure, exceeding both the PBR and equilibrium and the impact is enhanced at higher pressure.

This results from a combination of faster kinetics, less constrained thermodynamics, and stronger permeation (Figure 1). Increasing from 10 - 30 *bar* results in nominally complete ammonia recovery, the permeate purity can be upgraded to over 30%, and importantly the ammonia fraction in the retentate is negligible, enabling direct recycle without further purification.

Lastly, we consider the impact of temperature on a CMR with these membrane properties operated at $P = 30 \ bar$ as shown in Figure 8. For a conventional PBR $400^{\circ}C$ is optimal, with performance constrained by kinetics at lower temperature and equilibrium at higher temperature. With efficient ammonia removal, conversion increases monotonically with temperature since equilibrium constraints are removed, as shown in Figure 8 (a). Notably, the conversion is 17.7% at a temperature as low as $300^{\circ}C$, and is higher than 14.5% in a PBR at $400^{\circ}C$. As temperature is further reduced to $250^{\circ}C$ kinetics become limiting and the benefits of using a CMR are attenuated. Ammonia recovery (Figure 8 b) is a weak function of temperature and dictated by pressure as discussed above. Figure 8 c plots the ammonia purity in both the permeate and retentate at various temperatures. The permeate purity increases with temperature, reflecting the higher levels of conversion. The ammonia purity in a CMR is at least 3X greater than what is expected from a conventional PBR operated at

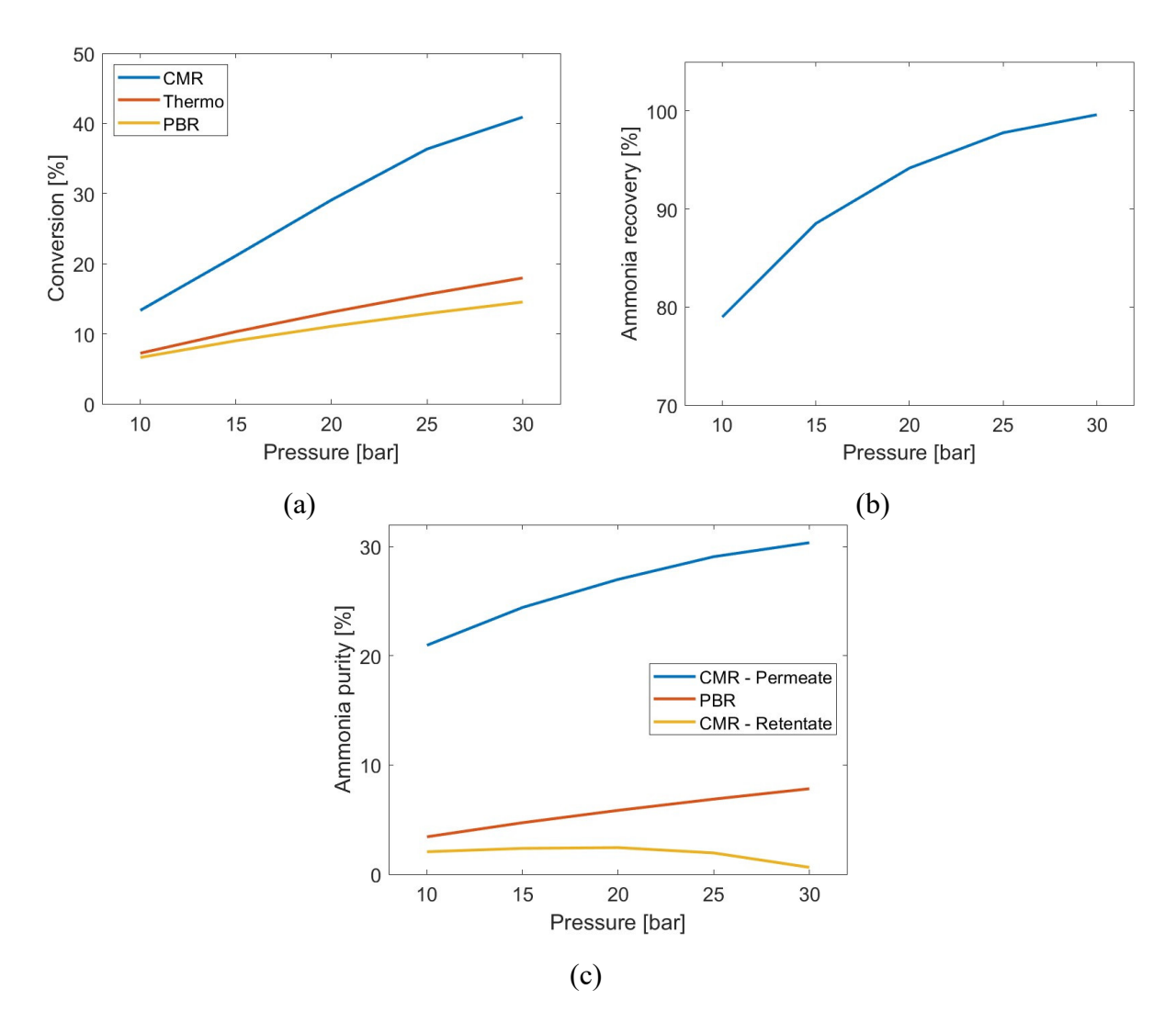


Figure 7: Conversion (a), ammonia recovery (b), ammonia purity (c) in the permeate and retentate as a function of pressure at $T = 400^{\circ}C$, H_2/N_2 ratio = 3, and $GHSV = 4000 \ h^{-1}$. The ammonia permeance, A/H and A/N selectivity are fixed at 1000 GPU, 10, and 100, respectively. Thermo represents equilibrium conversion.

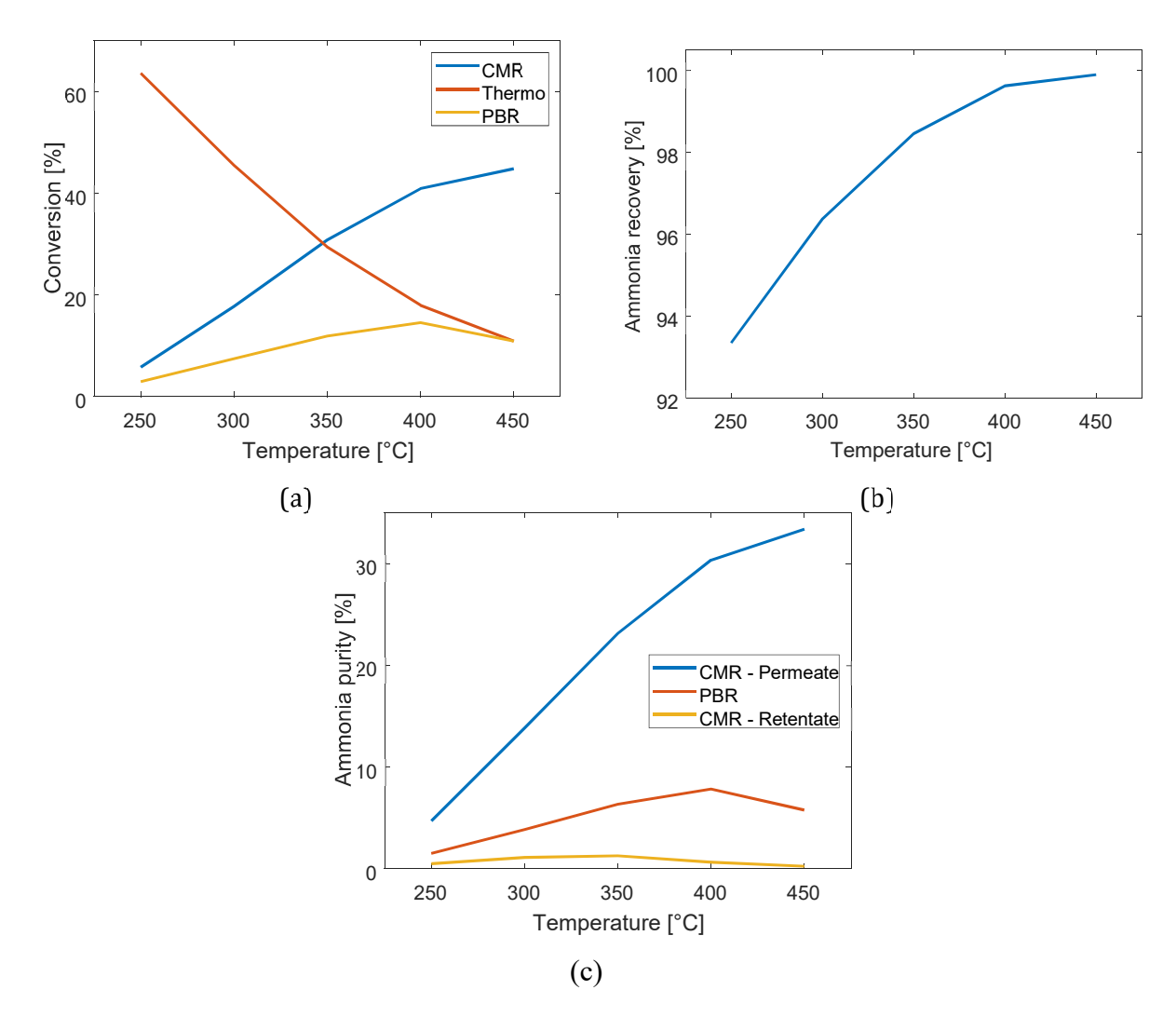


Figure 8: Conversion (a), ammonia recovery (b), ammonia purity (c) in the permeate and retentate as functions of temperature) at $P = 30 \ bar$, H_2/N_2 ratio = 3, and $GHSV = 4000 \ h^{-1}$. The ammonia permeance, A/H and A/N selectivity are fixed at 1000 *GPU*, 10, and 100, separately. Thermo represents equilibrium conversion.

these conditions. With a high permeance membrane such as this the level of ammonia in the retentate stream is negligible, enabling direct recycle of this stream to the reactor without the need for purification or recompression.

Candidates for ammonia permeable membranes

Previously, the benefits of CMRs have been demonstrated against PBRs mainly for dehydrogenation processes such as ammonia decomposition^{21,33} and steam methane reforming.³⁴ These successful implementations rely heavily on well-developed hydrogen-permeable membranes based on Pd and Pd alloys. 35 Likewise, ammonia permeable membranes are crucial to successfully developing CMR technology for ammonia synthesis. Table 4 summarizes the performance of ammonia permeable membranes from the literature. For separating ammonia from nitrogen and hydrogen, the majority of work to date has focused on polymeric membranes that operate via a diffusion-solubility mechanism, ²⁶ where the introduction of functional groups with high ammonia solubility enable selective permeation over hydrogen and nitrogen. Laciak et al.²⁹ and Bhown et al.²⁶ immobilized ammonium thiocyanate using poly(vinylamine) and porous Nylon as the membrane backbone, obtaining permeance up to 1900 GPU and very high selectivity over both hydrogen and nitrogen (~ 3000) at a temperature of $20^{\circ}C$ and pressures up to $\sim 66 \ bar$. However, the permeance drops to 30 GPU at increased temperature of 110 °C. Tricoli et al.³⁰ further improved the ammonia permeance by fabricating thin, 1.9 μ m Nafion coated microporous polypropylene hollow fiber membranes. Although high ammonia permeance and selectivity have been achieved in organic membranes, their thermal stability precludes deployment in a CMR at practical operating temperatures (300 - $450^{\circ}C$).

Table 4: Summary of ammonia permeable membranes in the literature. The results are presented using the highest operating temperature reported and the corresponding permeance, A/N selectivity, and A/H selectivity.

Membrane material	Highest operating temperature [°C]	Permeance [GPU]	A/N selectivity	A/H selectivity	References
Ammonium thiocyanate	50	180	1000	N/A	28
Poly(vinylammoniu m Thiocyanate)	73	160	>1000	N/A	29
Poly(vinylammoniu m Thiocyanate)	110	30	>3000	>3000	26
Nafion	180	1370	>2000	>600	30
MFI zeolite	80	639	14	9	31
Silica	80	2275	14	7	31
Silica	400	3760	N/A	0.083	32
LiNO ₃	279	50	245	N/A	27
$ZnCl_2$	350	700	>1000	>3000	27
ZIF-21	25	~1000	~25	~10	38

Inorganic ammonia permeable membranes have the potential to operate at synthesis temperatures, but there has been very limited work reported to date. Zeolite³¹ and silica membranes³² in principal could work via molecular sieving, as the kinetic diameter of NH₃ (2.6 °A) is reported to be smaller than both H₂ (2.9 °A) and N₂ (3.6 °A). These membranes have exhibited high permeance (> 100 GPU), but have only demonstrated reasonable selectivity (~ 10) at low temperature (< 100°C). The selectivity mechanism was attributed to preferential adsorption of ammonia that impedes H₂/N₂ transport.³² A second strategy for inorganic membranes is based on molten salts such as LiNO₃ and ZnCl₂ immobilized within a porous support.²⁷ The ammonia permeance of ZnCl₂ membranes increased from 500 to 700 GPU at temperatures from 250 to 350°C, and the selectivity of NH₃ over N₂ and H₂ exceed 3000 and 1000, respectively. These membranes work though a facilitated transport mechanism, and as such the ammonia permeance was found to scale inversely with the ammonia feed partial pressure. ^{27,30} Very recently³⁸ our group has introduced membranes based on zeolitic imidazolate framework (ZIF) that display permeance values >1000 GPU and ideal selectivity for NH₃ over N₂ and H₂ up to 35 and 12, respectively. Initial testing was done at ambient temperature but this class of materials is thermally stable up to $>300^{\circ}$ C.

Ammonia permeable membranes have been proposed as a separator before the refrigeration unit. 36,37 However, to the authors' knowledge, this work is the first to explore the use of the CMR for ammonia synthesis. The results obtained in this study suggest that CMR technology could be an attractive technology for distributed ammonia production at low temperature and modest pressure, provided that sufficient membrane technologies are available. While the membrane requirements identified in this work are challenging they are not beyond the realm of possibility. Laciak et al. 27 have demonstrated excellent ammonia permeance up to 700 *GPU* and A/N and A/H selectivity at least 1000 and 3000 using immobilized ZnCl₂ molten salt membranes at T = $350^{\circ}C$.

A drawback of this technology is that the ammonia permeance drops by up to 80% after increasing the ammonia feed partial pressure from 0.1 *bar* to 1 *bar*. While this presents a reactor engineering challenge, a CMR with high ammonia permeance can maintain the low ammonia partial pressure allowing such a membrane to retain sufficient performance. Additionally, the recently discovered ZIF based membranes³⁸ offer the potential to meet the performance requirements established herein. A final caveat is that the simulations discussed above assumed vacuum or an inert sweep gas on the permeate side to simplify the calculations. This maximizes the potential driving force for permeation and enables the possibility of complete ammonia recovery. In reality the permeate would likely be collected at atmosphere or potentially elevated pressure to facilitate its liquefaction. Thus the predictions for ammonia recovery are overly optimistic, but operation at 30 *bar* would be expected to provide a sufficient driving force to enable significant if not complete recovery. An optimal permeate pressure needs to be selected considering the membrane's ammonia permeance and effective selectivity by integrating the CMR model with a more complete process simulation.

Summary and conclusions

A reactor model was developed for CMR production of ammonia that employed a validated kinetic model based on current industrial catalysts and considered the impact of membrane properties, pressure, and temperature. The model identified minimum material requirements, and the key conclusions for each parameter are summarized below:

- Ammonia Permeance: Permeance is critical to both conversion and recovery. Membranes must have a permeance $> 100 \ GPU$ in order to realize significant benefits, and these improvement scales with permeance up to $1000 \ GPU$. Above this value further gains saturate.
- Selectivity: The benefits of permeance described above require minimum values of selectivity. Ideally, selectivity over both N_2 and H_2 should be > 10, but the minimum requirements were A/H > 4 and A/N > 10. Above the S = 10 threshold, the degree of conversion and recovery is generally independent of selectivity. In contrast, permeate purity scales sharply with the effective selectivity, where the lower of the two values is controlling.
- Pressure has a dramatic positive impact as it drives permeation, kinetics, and thermodynamics. Conversion scales linearly with pressure and operation at 30 *bar* is sufficient as ammonia recovery approaches 100%, and the ammonia concentration in the retentate becomes negligible, enabling direct recycling to the reactor without additional purification or recompression.
- Temperature has a negligible impact on recovery or purity, which are dictated by pressure and membrane properties, respectively. The main impact is conversion, and with the membrane removing equilibrium constraints conversion increases monotonically with temperature. Alternatively, a CMR could operate at 300°C with performance in excess of a conventional PBR operated at 400°C.

Nomenclature

Physical quantity

- A Pre-exponential factor
- A_m Surface area of the membrane for permeation
- E_a Activation energy [kJ mol]
- F Flow rate [sccm]
- $F_{m/g}$ Factor that represents the ratio of the surface area of the membrane to the volume of the reactor
- J Permeation flux by membrane separation [$mol\ cm^{-2}\ s^{-1}$]
- K_1 Equilibrium constant for the nitrogen adsorption step [bar]
- k_2 Forward rate constant for the nitrogen dissociation step $[bar^{-2}s^{-1}]$
- K_a Equilibrium constant for the surface reaction step $[bar^{-0.5}]$
- K_b Equilibrium constant for the hydrogen adsorption and dissociation step [$bar^{0.5}$]
- K_g Total number of gas species
- K_{eq} Equilibrium constant for the global synthesis reaction [bar^{-2}]
- L Length of the tubular reactor [cm]
- N_s Active sites density [$\mu mol\ gcat^{-1}$]
- P Pressure [bar], 1 bar = 0.1 MPa
- R Universal gas constant $[J mol^{-1} K^{-1}]$

- *r* Radii of the tubular reactor [*cm*]
- r_{NH3} Synthesis rate by catalyst mass [$\mu mol\ gcat^{-1}\ s^{-1}$]
- Re_r Reynolds number based on the radii of the reactor
- S Selectivity
- Sc Schmidt number
- T Temperature [K]
- u Mass averaged mean velocity [$cm s^{-1}$]
- W Molecular weight $[g mol^{-1}]$
- Y Mass fraction
- z Axial distance [cm]

Greek letters

- β H₂/N₂ ratio
- γ Stoichiometric coefficient
- κ Permeance [GPU], 1 GPU = 3.4 × 10⁻¹⁰ mol m⁻²s⁻¹ Pa⁻¹
- ρ Density $[g cm^{-3}]$
- θ_* Fraction of the surface coverage for free sites

Subscript

- A/H Ammonia over hydrogen
- A/N Ammonia over nitrogen
- k Species k
- H_2 Hydrogen
- N₂ Nitrogen
- *NH*₃ Ammonia
- per Permeate side

ret Retentate side

References

- 1. International Energy Agency. Renewables Information. 2020.
- 2. Kroposki B. Integrating high levels of variable renewable energy into electric powersystems.

 Journal of Modern Power Systems and Clean Energy. 2017;5(6):831–837.
- 3. Klerke A, Christensen CH, Nørskov JK, Vegge T. Ammonia for hydrogen storage: challenges and opportunities. Journal of Materials Chemistry. 2008;18(20):2304–2310.
- 4. Apodaca L. Nitrogen. report U.S. Department of the Interior, U.S. Geological Survey2017.
- Hoeven M, Kobayashi Y, Diercks R. Technology roadmap: Energy and GHG reductions in the chemical industry via catalytic processes. International Energy Agency: Paris.
 2013;56.
- 6. Reese M, Marquart C, Malmali M, et al. Performance of a small-scale Haber process. Industrial & Engineering Chemistry Research. 2016;55(13):3742–3750.
- Zhang Z, Karakaya C, Kee RJ, Way JD, Wolden CA. Barium-promoted ruthenium catalysts on yittria-stabilized zirconia supports for ammonia synthesis. ACS Sustainable Chemistry & Engineering. 2019;7(21):18038–18047.
- 8. Rosowski F, Hornung A, Hinrichsen O, Herein D, Muhler M, Ertl G. Ruthenium catalysts for ammonia synthesis at high pressures: Preparation, characterization, and power-law kinetics. Applied Catalysis A: General. 1997;151(2):443–460.
- 9. Kitano M, Inoue Y, Yamazaki Y, et al. Ammonia synthesis using a stable electride as an electron donor and reversible hydrogen store. Nature chemistry. 2012;4(11):934–940.
- 10. Smith C, McCormick AV, Cussler E. Optimizing the conditions for ammonia production using absorption. ACS Sustainable Chemistry & Engineering. 2019;7(4):4019–4029.
- 11. Palys MJ, McCormick A, Cussler E, Daoutidis P. Modeling and optimal design of absorbent enhanced ammonia synthesis. Processes. 2018;6(7):91.

- 12. Malmali M, Le G, Hendrickson J, Prince J, McCormick AV, Cussler E. Better absorbentsfor ammonia separation. ACS Sustainable Chemistry & Engineering. 2018;6(5):6536–6546.
- 13. Ojha DK, Kale MJ, McCormick AV, et al. Integrated Ammonia Synthesis and Separation. ACS Sustainable Chemistry & Engineering. 2019;7(23):18785-18792.
- 14. Malmali M, Wei Y, McCormick A, Cussler EL. Ammonia synthesis at reduced pressure via reactive separation. Industrial & Engineering Chemistry Research. 2016;55(33):8922–8932.
- 15. Hagen S, Barfod R, Fehrmann R, Jacobsen CJ, Teunissen HT, Chorkendorff I. Ammonia synthesis with barium-promoted iron–cobalt alloys supported on carbon. Journal of Catalysis. 2003;214(2):327–335.
- 16. Sehested J, Jacobsen CJ, T¨ornqvist E, Rokni S, Stoltze P. Ammonia synthesis over a multipromoted iron catalyst: extended set of activity measurements, microkinetic model, and hydrogen inhibition. Journal of Catalysis. 1999;188(1):83–89.
- 17. Scholten J. An investigation on promoted iron catalysts for the synthesis of ammonia: By Anders Nielsen. Jul. Gjellerups Forlag, Copenhagen, 1968. 263 pp. Price: Da. Cr. 28, paperbound; Da. Cr. 36, clothbound (excl. Danish sales tax). 1968.
- 18. Kowalczyk Z. Effect of potassium on the high pressure kinetics of ammonia synthesis over fused iron catalyst. Catalysis letters. 1996;37(3-4):173–179.
- 19. Collins JP, Way JD. Preparation and characterization of a composite palladium-ceramic membrane. Industrial & engineering chemistry research. 1993;32(12):3006–3013.
- 20. Raja LL, Kee RJ, Deutschmann O, Warnatz J, Schmidt LD. A critical evaluation of Navier–Stokes, boundary-layer, and plug-flow models of the flow and chemistry in a catalytic-combustion monolith. Catalysis Today. 2000;59(1-2):47–60.

- 21. Zhang Z, Liguori S, Fuerst TF, Way JD, Wolden CA. Efficient ammonia decomposition in a catalytic membrane reactor to enable hydrogen storage and utilization. ACS Sustainable Chemistry & Engineering. 2019;7(6):5975–5985.
- Appl M. Ammonia: Principles and industrial practice. Vch Verlagsgesellschaft Mbh
 1999.
- 23. Arau'jo A, Skogestad S. Control structure design for the ammonia synthesis process. Comput. Chem. Eng.. 2008;32:2920-2932.
- 24. Tosti S, Basile A, Borelli R, et al. Ethanol steam reforming kinetics of a Pd–Ag membrane reactor. International journal of hydrogen energy. 2009;34(11):4747–4754.
- 25. Breck DW. Zeolite molecular sieves: structure, chemistry and use. Krieger 1984.
- Bhown A, Cussler E. Mechanism for selective ammonia transport through poly (vinylammonium thiocyanate) membranes. Journal of the American Chemical Society.
 1991;113(3):742–749.
- 27. Laciak DV, Pez GP, Burban PM. Molten salt facilitated transport membranes. Part 2. Separation of ammonia from nitrogen and hydrogen at high temperatures. Journal of membrane science. 1992;65(1-2):31–38.
- 28. Pez GP, Laciak DV. Ammonia separation using semipermeable membranes. 1988. US Patent 4,762,535.
- Laciak DV, Pez GP. Ammonia separation using ion exchange polymeric membranes and sorbents.
 1988. US Patent 4,758,250.
- 30. Tricoli V, Cussler E. Ammonia selective hollow fibers. Journal of membrane science. 1995;104(1-2):19–26.
- 31. Camus O, Perera S, Crittenden B, et al. Ceramic membranes for ammonia recovery. AIChE journal. 2006;52(6):2055–2065.

- 32. Kanezashi M, Yamamoto A, Yoshioka T, Tsuru T. Characteristics of ammonia permeation through porous silica membranes. AIChE journal. 2010;56(5):1204–1212.
- 33. Li G, Kanezashi M, Yoshioka T, Tsuru T. Ammonia decomposition in catalytic membrane reactors: simulation and experimental studies. AIChE Journal. 2013;59(1):168–179.
- 34. El Hawa HWA, Lundin STB, Patki NS, Way JD. Steam methane reforming in a PdAu membrane reactor: Long-term assessment. international journal of hydrogen energy. 2016;41(24):10193–10201.
- 35. Paglieri S, Way J. Innovations in palladium membrane research. Separation and Purification Methods. 2002;31(1):1–169.
- 36. Bikson B, Nelson JK, Perrin JE. Process for recovery of ammonia from an ammonia containing gas mixture. 1991. US Patent 5,009,678.
- 37. Choe JS, Kellogg Jr LJ. Membrane-assisted process to produce ammonia. 1995. US Patent 5,455,016.
- 38. Wei Q, Lucero JM, Crawford JM, Way JD, Wolden CA, Carreon MA, "Ammonia separation from N₂ and H₂ over LTA zeolitic imidazolate framework membranes, Journal of Membrane Science.2021 119078. In press https://doi.org/10.1016/j.memsci.2021.119078

FIGURE CAPTIONS

Figure 1: Equilibrium conversion of stoichiometric N₂:H₂ mixtures as a function of temperature at selected pressures.

Figure 2: Comparison of ammonia outlet concentration in an integral reactor between experimental results and model predictions of bulk iron catalysts at $T = 400^{\circ}C$ and $P = 1 \ bar^{8}$, $2 \ bar^{17}$, $10 \ bar^{15}$, $100 \ bar^{18}$, $107 \ bar^{8}$.

Figure 3: Conversion vs. pressure at various GHSV for the base case of a PBR with no permeation at $T = 400^{\circ}C$. At GHSV $\leq 1000 \text{ h}^{-1}$ equilibrium conversion is obtained.

Figure 4: Conversion as a function of ammonia selectivity over nitrogen and hydrogen at ammonia permeance levels of (a) 10, (b) 100, and (c) 1000 *GPU* with other conditions fixed at $T = 400^{\circ}C$, $P = 10 \ bar$, H_2/N_2 ratio = 3, and $GHSV = 4000 \ h^{-1}$. PBR conversion (6.6%) represents the packed bed reactor with no membrane separation. Equilibrium conversion is 7.2% at these conditions. Note that in Fig. 4c the results are cut off below A/H = 5 due to numerical instabilities encountered.

Figure 5: Ammonia recovery as a function of ammonia selectivity over nitrogen and hydrogen at ammonia permeance levels of (a) 10, (b) 100, and (c) 1000 *GPU* with other conditions fixed at T = $400^{\circ}C$, P = $10 \ bar$, H₂/N₂ ratio = 3, and GHSV = $4000 \ h^{-1}$ (d) Ammonia recovery as a function of Pe number assuming perfect A/N and A/H selectivities at T = $400^{\circ}C$, P = $10 - 30 \ bar$, H₂/N₂ ratio = 3, GHSV = $4000 \ h^{-1}$, and ammonia permeance values are within $10 - 1000 \ GPU$.

Figure 6: Permeate purity as a function of ammonia selectivity over nitrogen and hydrogen at ammonia permeance levels of (a) 10, (b) 100, and (c) 1000 *GPU* with other conditions fixed at T = $400^{\circ}C$, P = $10 \ bar$, H₂/N₂ ratio = 3, and GHSV = $4000 \ h^{-1}$. The purity exiting a PBR is 3.4% at these conditions. (d) Permeate purity plotted vs. effective selectivity from these simulations (a-c).

Figure 7: Conversion (a), ammonia recovery (b), ammonia purity (c) in the permeate and retentate as a function of pressure at $T = 400^{\circ}C$, H_2/N_2 ratio = 3, and $GHSV = 4000 \ h^{-1}$. The ammonia permeance, A/H and A/N selectivity are fixed at 1000 GPU, 10, and 100, respectively. Thermo represents equilibrium conversion.

Figure 8: Conversion (a), ammonia recovery (b), ammonia purity (c) in the permeate and retentate as functions of temperature) at $P = 30 \ bar$, $H_2/N_2 \text{ ratio} = 3$, and $GHSV = 4000 \ h^{-1}$. The ammonia permeance, A/H and A/N selectivity are fixed at 1000 *GPU*, 10, and 100, separately. Thermo represents equilibrium conversion.

Table 1: Summary of kinetic parameters including values and units for Eq. 2

Kinetic	Units	Pre-exponential factor A	Activation energy E_a
parameters			$[kJ mol^{-1}]$
$2NsK_1k_2$	$[\mu mol\ gcat^{-1}s^{-1}bar^{-1}]$	7.80×10^{3}	6.6
K_{eq}	$[bar^{-2}]$	2.03×10^{-12}	-101.6
K_a	$[bar^{-0.5}]$	2.73×10^{-2}	27.1
K_b	$[bar^{0.5}]$	2.16×10^{3}	48.0

Table 2: Summary of the reactor model setup.

Parameters	Values
L[cm]	20
r[cm]	0.5
Permeation area $A_m[cm^2]$	62.8
Valid GHSV range $[h^{-1}]$	8 - 12,800
Catalyst density [g cm ⁻³]	4.8
Catalyst porosity	0.44
Catalyst bed voidage	0.33

Table 3: Summary of the parameter space.

Parameter	Values
Temperature [$^{\circ}C$]	250 - 450
Pressure [bar]	10 - 30
H ₂ /N ₂ ratio	3
GHSV $[h^{-1}]$	1000 - 8000
NH ₃ permeance [GPU]	10 - 1000
A/N selectivity	1 - 1000
A/H selectivity	1 - 1000

Table 4: Summary of ammonia permeable membranes in the literature. The results are presented using the highest operating temperature reported and the corresponding permeance, A/N selectivity, and A/H selectivity.

Membrane material	Highest operating temperature [°C]	Permeance [GPU]	A/N selectivity	A/H selectivity	References
Ammonium thiocyanate	50	180	1000	N/A	28
Poly(vinylammonium Thiocyanate)	73	160	>1000	N/A	29
Poly(vinylammonium Thiocyanate)	110	30	>3000	>3000	26
Nafion	180	1370	>2000	>600	30
MFI zeolite	80	639	14	9	31
Silica	80	2275	14	7	31
Silica	400	3760	N/A	0.083	32
LiNO ₃	279	50	245	N/A	27
$ZnCl_2$	350	700	>1000	>3000	27
ZIF-21	25	~1000	~25	~10	38